SCIENTIFIC REPORTS

Gassing in $Li_4Ti_5O_{12}$-based batteries and its remedy

Yan-Bing He[1,2], Baohua Li[1], Ming Liu[1], Chen Zhang[3], Wei Lv[1,3], Cheng Yang[1], Jia Li[1], Hongda Du[1], Biao Zhang[2], Quan-Hong Yang[1,3], Jang-Kyo Kim[2] & Feiyu Kang[1]

[1]Engineering Laboratory for Functionalized Carbon Materials and Key Laboratory of Thermal Management Engineering and Materials, Graduate School at Shenzhen, Tsinghua University, Shenzhen 518055, China, [2]Department of Mechanical Engineering, Hong Kong University of Science and Technology, Clear Water Bay, Kowloon, Hong Kong, [3]School of Chemical Engineering and Technology, Tianjin University, Tianjin 300072, China.

Destructive gas generation with associated swelling has been a major challenge to the large-scale application of lithium ion batteries (LIBs) made from $Li_4Ti_5O_{12}$ (LTO) anodes. Here we report root causes of the gassing behavior, and suggest remedy to suppress it. The generated gases mainly contain H_2, CO_2 and CO, which originate from interfacial reactions between LTO and surrounding alkyl carbonate solvents. The reactions occur at the very thin outermost surface of LTO (111) plane, which result in transformation from (111) to (222) plane and formation of (101) plane of anatase TiO_2. A nanoscale carbon coating along with a stable solid electrolyte interface (SEI) film around LTO is seen most effective as a barrier layer in suppressing the interfacial reaction and resulting gassing from the LTO surface. Such an ability to tune the interface nanostructure of electrodes has practical implications in the design of next-generation high power LIBs.

L ithium ion batteries (LIBs) have been widely applied in many electronic devices due to their high energy densities, flexible design, light weight and long lifespan compared to other types of batteries, such as Ni-Cd, Ni-MH and lead acid batteries[1,2]. For the same reasons, they also have been considered as an excellent power source for electric vehicles (EVs) and energy storage stations (ESSs) that require high energy density, long cyclic life and excellent safety performance. At present, various forms of carbons are the dominant source of anode materials for LIBs[3,4], which, however, have shown some critical issues, including poor cyclic life, high reactivity with electrolyte solution that easily contribute to the thermal runaways of battery under certain abusive conditions[5]. Myriad investigations have hitherto been conducted to develop new electrode materials that possess much improved electrochemical and safety performance[6–8].

Spinel $Li_4Ti_5O_{12}$ (LTO) anode has a theoretical capacity of 175 mAhg^{-1} within the voltage range of 2.5~1.0 V, and exhibits excellent reversibility due to its zero volume change during charge/discharge cycles. In addition, LTO demonstrates excellent safety and cyclic performance, making it a potential anode material for high power applications[9–11]. Unfortunately, LTO shows a low intrinsic electronic conductivity and lithium-ion diffusion coefficient[12,13], resulting in poor high-rate charge/discharge capabilities. A number of strategies, including carbon coating[14,15], metal and nonmetal ion doping[13,16–18], hybridization with carbon and metal powders[19–23], reduction in particle size[24], and formation of micro-scale secondary particles consisting of nanostructured primary particles[8,13], have been devised to improve the electrochemical performance of LTO anodes with varied success.

Even after a decade of tremendous efforts based on the above approaches[25], however, LTO anode is not considered the most preferable choice for large-scale applications by the power LIB industries mainly due to severe gassing during charge/discharge cycles and storage, especially at elevated temperatures[26,27]. Gassing in lead-acid batteries is known to be caused by overcharging or short circuits inside the battery[28,29]. However, gassing in LTO-based LIBs is little understood although it leads to serious swelling and hence becomes a grave safety concern, a main obstacle to widespread use of LTO-based batteries. The battery industries are expecting an effective remedy for the gassing problem so as to pave the way for the vast applications of LTO power battery in EVs and ESSs. To date, there are only a few reports that specifically refer to the gassing behavior of LTO electrodes[26,27,30–32]. Very recently, the gas generated inside the LTO/$LiMn_2O_4$ cells has been confirmed to mainly consist of H_2, CO_2 and CO[26]. It is suggested that H_2 is possibly derived from a trace of H_2O, while CO and CO_2 result from the decomposition of electrolyte solution initiated at relatively high temperatures by PF_5 that is a strong Lewis acid and one of the decomposition products of the electrolyte, $LiPF_6$[26,33–35]. However, gassing always occurs even when the LTO-based battery is not cycled and only stored at room temperature. Moreover, commercial graphite anodes soaked in $LiPF_6$ electrolyte do not show similar gassing behavior during storage or cyclic

test under similar conditions. The above literature survey and practical operational experience clearly indicate that the underlying mechanisms for the formation of these gasses are still unclear, and the understanding of the roles of $LiPF_6$ electrolyte in gassing reactions in LTO-based batteries is far from complete.

Here we aim to identify the root causes of gassing in LTO-based batteries, and hence to propose effective methods to control it. For these purposes, we designed five experimental conditions (see Table 1 for details). Conditions A, B and C are intended to identify whether the gassing reactions are initiated by PF_5 or LTO. Conditions D and E, which are encountered in the practical operation of LIBs, are respectively employed to evaluate gas generation process during storage (fully charged in the formation process) and cyclic tests of soft-packed LTO batteries. The comparative investigations on the above five conditions help reach an understanding of the root causes of the gassing behaviors, that is, interfacial reaction between LTO and electrolyte solution; note that not PF_5 but LTO initiates such an interfacial reaction based the gassing process associated with a phase change and the formation of a new phase; and a carbon coating, functioning as a constructive barrier around LTO particles, is effective to suppress the gassing and the resultant swelling of commercial LTO-based batteries.

Results

Gassing behaviors under Conditions A–E. Nano-structured active materials have a high reactivity with electrolyte, making it very difficult to detect the intrinsic reactions taking place between the electrode and electrolyte. Therefore, micro-sized cubic LTO powders were synthesized to study the gassing reactions in this work. The particle size of LTO is ~1 μm as confirmed by the scanning electron microscopy (SEM) and transmission electron microscopy (TEM) observations (Supplementary Fig. S1a–b). The X-ray diffraction (XRD) patterns of the LTO is in good agreement with the JCPDS standard (card No. 49-0207) and can be indexed to the spinel structure of LTO with the space group $Fd3m$ (Supplementary Fig. S1c). Weak diffraction peaks of rutile TiO_2 are detected, indicating an existence of small fraction of rutile TiO_2 nano-coating that can improve the rate performance of LTO[36].

The soft packed NCM/LTO batteries were assembled with $Li(Ni_{1/3}Co_{1/3}Mn_{1/3})O_2$ (NCM) as the cathode, the LTO prepared above as the anode, and 1 M $LiPF_6$/EC+DMC+EMC as the electrolyte solution. Using such soft packed NCM/LTO batteries, the specific capacities of the LTO measured at the 1st and 400th cycles are 148.7 and 138.5 mAh g^{-1}, respectively (Fig. 1a). It is noted that very obvious swelling is observed for the battery after cyclic test under Condition E (Fig. 1e–f). Even the fully charged battery that was only stored at 25°C for 3 months (Conditions D) also presents similar gassing behavior (Fig. 1c–d). It is apparent that the swelling results from the gas generated in the soft packed batteries. The rate of gassing gradually decreases with increasing the storage and cyclic period.

As presented above, five conditions were designed to simulate the gassing process between LTO and electrolyte (See Table 1 for details). Interestingly, obvious swelling also occur when LTO or rutile TiO_2 is soaked in solvents (Condition A) or electrolyte solution (Condition B) (not subject to any electrochemical process), whereas there is no obvious swelling when there is only electrolyte solution in the absence of LTO or rutile TiO_2 (Condition C). This difference can be clearly identified from the volume of gas generated under Conditions A, B and C (Fig. 2e). The above results indicate that the gassing behaviors are intimately related to LTO or rutile TiO_2.

The gas components were analyzed by gas chromatograms and the results are summarized in Table 2 and Table S1. The gassing behaviors of LTO with electrolyte solution or solvent under different conditions are schematically depicted in Fig. 2a–d. CO_2 is the only component generated when LTO is soaked under Conditions A and B, whereas H_2, CO_2, CO and a trace of gaseous hydrocarbons are generated when the NCM/LTO batteries are stored (Condition D) and cycled (Condition E) where H_2 fraction is over 50 wt%. Note that H_2 and CO are generated in the batteries that were subjected to charge/discharge cyclic test, suggesting that the charged LTO promotes the generation of H_2 and CO which are driven by electrochemical reactions.

PF_5, a strong Lewis acid and one of the decomposition products of $LiPF_6$, has been mistakenly considered as the major source of initiating the gassing reactions in the presence of trace amount of water[26,33]. In sharp contrast, our observation indicate that gassing always occurs even when LTO is soaked in solvents under Condition A (totally free from $LiPF_6$) and CO_2 is the only gas component (Fig. 2e and Supplementary Table S1). That is to say that PF_5 originated from $LiPF_6$ is not mainly responsible for the generation of CO_2[33,34]. As discussed above, much less gassing occurs under Condition C (totally free from LTO or rutile TiO_2) as compared to the cases under Conditions A and B. It is therefore concluded that CO_2 generation is mainly attributed to the intrinsic reaction between LTO or rutile TiO_2 and alkyl carbonate solvents. Unexpectedly, the volume of gas generated of LTO or rutile TiO_2 soaked under Condition A is obviously larger than that under Condition B, although the component of gas is exactly the same (CO_2) (Fig. 2e). This further indicates that $LiPF_6$ does not favor the gassing reactions, but rather suppresses it to a certain extent (details will be discussed below).

As is expected, the reactivity of solvents and electrolyte solutions with LTO or rutile TiO_2 at 50°C is higher than that at 25°C, which suggests that the higher temperature also promote the above reactions. This can explain why the LTO-based battery is easily swelling at high temperature. For the same reason, we discuss in details the LTO soaked in solvent or electrolytes at 50°C to image the gassing behaviors more distinctly.

The volume of the generated gas as demonstrated in Fig. 2e also indicates that the reactivity of rutile TiO_2 with electrolyte is apparently lower than that of LTO counterpart. In view of the above findings and a very small amount of rutile TiO_2 contained in LTO, the

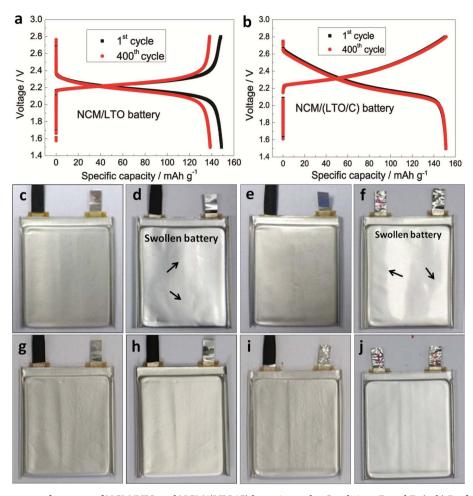| Table 1	Conditions A-E to study gassing reaction mechanisms of LTO electrodes	
Conditions		**Remarks**
Condition A	Package containing LTO (or rutile TiO_2) soaked in electrolyte-free solvents at 25 or 50°C for 3 months	Ethylene carbonate (EC); Diethyl carbonate (DEC); Dimethyl carbonate (DMC); Ethylene methyl carbonate (EMC); Propylene carbonate (PC)
Condition B	Package containing LTO (or rutile TiO_2) soaked in electrolyte solution at 25 or 50°C for 3 months	1 M $LiPF_6$/EC; $LiPF_6$/DEC; $LiPF_6$/DMC; $LiPF_6$/EMC; $LiPF_6$/PC; $LiPF_6$/EC+DMC+EMC
Condition C	Electrolyte solution stored at 25 or 50°C for 3 months in absence of LTO	1 M $LiPF_6$/EC+DMC+EMC
Condition D	Fully charged soft-packed battery stored at 25°C for 3 months	NCM/LTO or NCM/(LTO/C) battery (see details in Experimental section) 1 M $LiPF_6$/EC+DMC+EMC is used as electrolyte solution
Condition E	Soft-packed battery cycled 400 times at 25°C at a charge/discharge rate of 0.5C	Same as Condition D

Figure 1 | Cyclic and storage performance of NCM/LTO and NCM/(LTO/C) batteries under Conditions D and E. (a, b) Performance curves at 0.5C/0.5C and 25°C (Condition E). Photographs of soft-packed NCM/LTO batteries (c) before and (d) after storage under Condition D, and (e) before and (f) after cyclic test under Condition E. Photographs of soft-packed NCM/(LTO/C) batteries (g) before and (h) after storage under Condition D, and (i) before and (j) after cyclic test under Condition E. Note that swelling caused by gassing is observed in the NCM/LTO batteries (arrows (↑) labels the obviously swollen areas), but not in the NCM/(LTO/C) batteries.

swelling of NCM/LTO batteries is mainly ascribed to the intrinsic reactions of LTO with electrolyte solution.

Carbon coating to suppress gassing in NCM/LTO battery. Here, carbon coating is employed as a thin barrier layer to control the gassing reaction by isolating the LTO particles from electrolyte solution. Carbon coated LTO (LTO/C) was prepared (see Methods) and its XRD pattern is in good agreement with the JCPDS file (card No. 49-0207) (Supplementary Fig. S3a). Low diffraction peaks of rutile and anatase TiO_2 are observed and LTO/C has a well-defined crystal structure with a particle size of around 300 nm (Supplementary Fig. S3b–e). The Raman spectra of LTO/C indicate that the carbon is mainly amorphous judging from the high the intensity ratio ($I_D/I_G=2.99$) of D- and G-band peaks (Supplementary Fig. S4a). Based on the thermogravimetric analysis (TGA), the carbon content is roughly estimated to be ~3.0 wt % (Supplementary Fig. S4b).

The soft-packed NCM/(LTO/C) batteries were prepared using LTO/C as the anode and the specific capacities measured after the 1st and 400th cycles at 0.5C/0.5C are 151.2 mAhg^{-1} and 151.3 mAhg^{-1}, respectively (Fig. 1b). These values present much higher cyclic stability than the corresponding values of the uncoated LTO (Fig. 1a), testament to the beneficial effect of the carbon coating. In particular, no visible swelling occurs for the LTO/C-based battery after storage and cyclic test under both Conditions D and E (Fig. 1g–j) unlike the uncoated LTO batteries (Fig.1c–f). This observation

suggests that the carbon coating is very effective in suppressing the gassing behavior of LTO batteries.

Note that both the LTO and LTO/C-based batteries were prepared using the same condition. No apparent gassing occurs in the LTO/C-based batteries, indicating that H_2 is not generated in the LTO/C-based batteries unlike the LTO-based batteries. This observation further hints that H_2 generated in LTO-base batteries is not caused by the reactions of Li ions (or Li metal) with the trace H_2O (or HF) that are present in both LTO-based and LTO/C-based batteries[33]. This means that the gassing based swelling of LTO-based batteries originates from the intrinsic reactions of electrolyte and LTO subjected to charge/discharge cyclic test.

Based on the above results, we can conclude that the gas generated in the swollen LTO-based batteries originates from the intrinsic reactions between the electrolyte solution and LTO, and is hardly related to PF_5 and H_2O. In the next section, the gassing reaction mechanisms of LTO with electrolyte solution under different conditions are discussed in more detail and the role of carbon coating in suppressing the gassing behavior of LTO batteries is elucidated.

Discussion

Gassing processes of LTO in presence of alkyl carbonate solvents under different conditions are discussed in details as follows. LTO soaking in electrolyte-free solvent (DEC as a typical solvent for Condition A) is discussed at first. The original LTO has a well-defined crystal structure as indicated by the high-resolution TEM
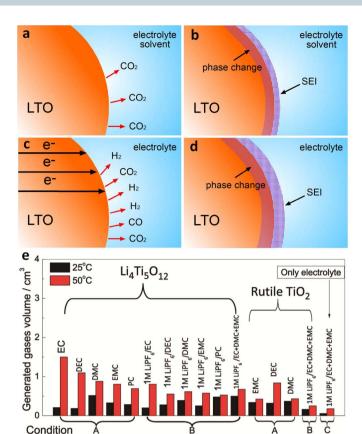
Figure 2 | Schematics of gassing behaviors of LTO electrodes with electrolyte under different conditions. (a) CO_2 is generated when LTO is soaked under Conditions A and B. (b) The surface of LTO is covered by solid electrolyte interface (SEI) film consisting of the reaction products of LTO with solvents or electrolyte solution, and the phase change occurs at the outermost surface of LTO soaked under Conditions A and B. Note that the components of SEI film formed under Conditions A and B is obviously different. (c) Gaseous H_2, CO_2 and CO are generated when NCM/LTO batteries are stored and cycled under Conditions D and E. (d) The surface of LTO is covered by a SEI film consisting of the reaction products of LTO with electrolyte under Conditions D and E, and phase change occurs at the outermost surface of LTO. Not that the thickness of SEI film under Conditions D and E are obviously different. (e) Volumes of gas generated when LTO or rutile TiO_2 is soaked under Conditions A, B and C.

(HRTEM) image (Fig. 3a), and the *d*-spacing of 0.489 nm is in agreement with that of the (111) plane of spinel LTO. After LTO was soaked in DEC (totally free from $LiPF_6$ as electrolyte), an apparent phase change occurs to the outermost surface and a very thin layer (3 nm in thickness) is unexpectedly formed around the LTO particles, which is totally different from the interior crystalline structure of the (111) plane (Fig. 3b)[32]. The *d*-spacing of the newly formed surface layer is 0.241 nm which matches well with that of the LTO (222) plane, indicating a transformation of the (111) plane to (222) plane at the outermost surface. Moreover, a new phase of the anatase TiO_2 (101) plane with d-spacing of 0.357 nm is observed

simultaneously (Fig. 3c). Judging from the absence of anatase TiO_2 in the as-prepared LTO, the anatase TiO_2 is also the result from soaking.

The Ti 2p and O 1s X-ray photoelectron spectroscopy (XPS) spectra of LTO obtained before and after soaking further prove the formation of TiO_2 (Supplementary Fig. S5b and g). The C 1s spectrum of LTO after soaking presents three small typical peaks at 285.4, 286.5 and 288.9 eV, which can be assigned to C-C, C-O and O-C=O groups (Supplementary Fig. S5l), respectively[37–39]. The peak assigned to lithium carbonates (Li_2CO_3 and $ROCO_2Li$) at 290.5 eV is not detected[38]. Furthermore, only CO_2 generated during soaking suggests that a decarboxylation reaction of DEC occurs at the interface between LTO and solvent.

The spinel crystallographic structure of LTO presents that the LTO (222) plane is composed only of $[Li_{1/3}Ti_{5/3}]$ layers, while the (111) plane is composed of Li^+, O^{2-} and $[Li_{1/3}Ti_{5/3}]$ ions layers (Supplementary Fig. S7a–g). The plane transformation of LTO from (111) to (222) and the formation of anatase TiO_2 suggest that the Li^+ and O^{2-} ions at outermost surface of LTO are taken away during the interfacial reaction between LTO and DEC, which is associated with the generation of CO_2 and the formation of a titanium-rich surface layer[32]. The XRD patterns suggest that LTO maintains its spinel structure after soaking (Supplementary Fig. S8b) and there are no obvious anatase TiO_2 peaks, indicating that only a very thin outermost surface layer of LTO takes part in the interfacial reaction and transforms to the anatase TiO_2 (101) plane.

Therefore, the above discussion suggests that the decarboxylation reaction associated with CO_2 generation is initiated by the terminated ions of LTO (111) plane, which results in the plane transformation from (111) to (222) and the formation of a new phase, anatase TiO_2 (101) plane. The possible reaction mechanism is described in Figure 4a[33]: the terminated Ti^{4+} ions of LTO coordinate with the unshared electron pairs of O^{2-} ions of carbonyl groups, while the outermost surface O^{2-} ions of LTO attack the carbon atom of CH_3CH_2O group and the flexible Li^+ ions coordinate with O^{2-} of CH_3CH_2O group. This reaction gives rise to the formation of CO_2, CH_3COOLi, anatase TiO_2 (101 plane) and $C_2H_5OC_2H_5$. The LTO is covered by a thin SEI film after soaking (Fig. 3b–c), which in turn separates the LTO from the surrounding DEC solvent and reduce to a certain extent the reactivity between LTO and solvent.

Similar gassing behaviors occur to LTO soaked in electrolyte solution (1 M $LiPF_6$/ EC+DMC+ EMC as an example for Condition B). The XRD pattern and HRTEM images show that the anatase TiO_2 (101) plane appeared in the LTO after soaking under Condition B (Figs 3d and 5c). However, both microstructure and surface chemistry of LTO are quite different under these two conditions (Supplementary Fig. S5h and 5m). Due to the existence of $LiPF_6$, Li_2TiF_6 (JCPDS file of card No. 24-0662) was formed as a result of the reactions between HF and LTO (or anatase TiO_2) (Fig. 5c)[26,40]. In addition, a large amount of LiF (JCPDS file of card No. 04-0857) was formed on the surface of LTO, arising from the decomposition of $LiPF_6$ at around 50°C. The LTO surface was covered by Li_2TiF_6 and LiF, making the reaction of LTO with surrounding solvents difficult. This is the main reason why the addition of $LiPF_6$ in the solvents reduces the reactivity of LTO with electrolyte and somewhat retards the gassing reactions.

Table 2 | Gas generated for LTO soaked under Conditions A and B, and NCM/LTO batteries stored and cycled under Conditions D and E, respectively

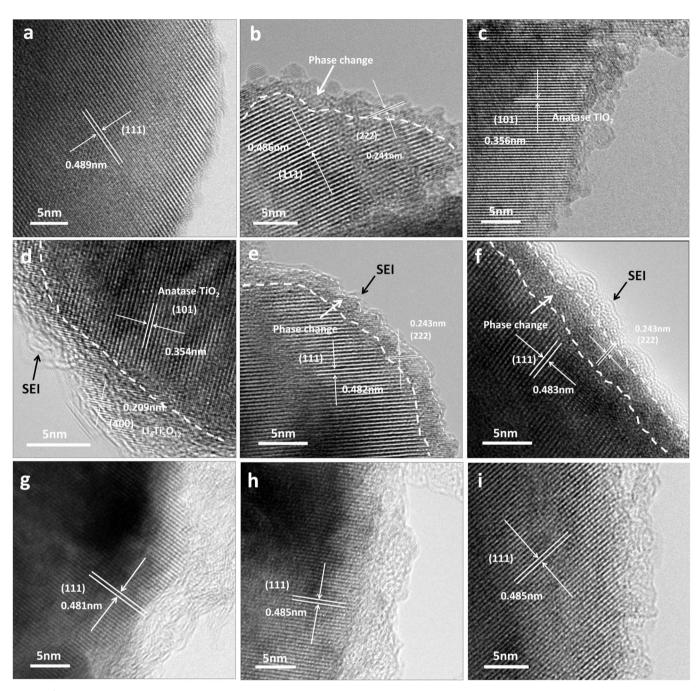|	CO_2 wt%	H_2 wt%	CO wt%	C_2H_4 wt%	C_2H_6 wt%	C_3H_8 wt%	CH_4 wt%
Condition A	100.00	/	/	/	/	/	/
Condition B	100.00	/	/	/	/	/	/
Condition D	30.41	55.65	10.00	2.09	1.10	0.32	0.43
Condition E	31.72	52.67	13.24	/	1.34	/	1.03

Figure 3 | TEM images of LTO and LTO/C electrodes. (a) As-prepared LTO. (b, c) LTO soaked under Condition A (DEC at 50°C). (d) LTO soaked under Condition B (1 M LiPF$_6$/EC+DMC+EMC at 50°C). (e) LTO in fully charged NCM/LTO battery stored under Condition D. (f) LTO in NCM/LTO battery cycled under Condition E. (g) As-prepared LTO/C. (h) LTO/C in fully charged NCM/(LTO/C) battery stored under Condition D. (i) LTO/C in NCM/(LTO/C) battery cycled under Condition E. Note that the LTO and LTO/C batteries tested under Conditions D and E were fully discharged before TEM examination.

The O 1s XPS profile presents a large peak at 532.4 eV which is assigned to C-O-C species, while two small peaks at 531.7 and 533.5 eV are attributed to the C=O species and the oxygen atom of lithium alkyl carbonates bounding to two carbon atoms, respectively[41,42] (Supplementary Fig. S5h). The C 1s detailed spectrum indicates that the C-O species are the main reaction products between LTO and electrolyte solution. The peaks assigned to carbonates are hardly detected (Supplementary Fig. S5m). The FTIR spectrum (Supplementary Fig. S6d) of LTO after soaking presents three main peaks at 1634, 1167 cm^{-1} and 1024 cm^{-1}, which are associated with C=O, C-O-C and ROLi species, respectively, and these results are in accordance with the XPS results. Only CO$_2$ is generated during LTO

soaking under Condition B as a result of the decarboxylation reactions of solvents, similarly to Condition A (DEC). These reactions are also associated with the removal of Li$^+$ and O^{2-} ions at the outermost surface of LTO leading to the formation of (222) plane and anatase TiO$_2$ (101) plane (Fig. 3d and Supplementary Fig. S8f). In view of the formation of many C-O-C species on the surface of LTO after soaking under Condition B, LTO may initiate the ring-opening polymerization of EC, which results in the formation of PEO-like oligomers (-CH$_2$-CH$_2$-O-)$_n$ and CO$_2$ (Figure 4b)[33,43].

The reacted surface of LTO is also covered by a SEI film with ~2 nm in thickness resulting from the interfacial reaction, which is much thicker than that of LTO soaked under Condition A

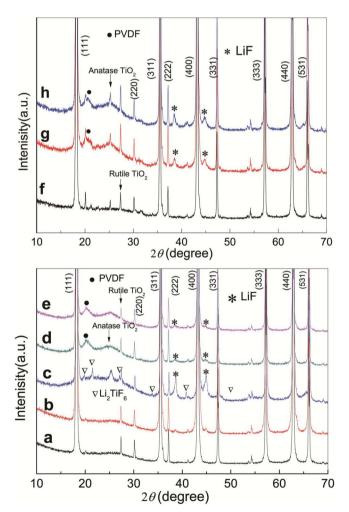**Figure 4 | Tentative gas generation reactions in the gassing of LTO electrode.**

Figure 5 | XRD patterns of LTO and LTO/C. (a) As-prepared LTO. (b) LTO after soaking under Condition A (DEC at 50°C). (c) LTO after soaking under Condition B (1 MLiPF$_6$/EC+DMC+EMC at 50°C). (d) LTO in fully charged NCM/LTO battery stored under Condition D. (e) LTO in NCM/LTO battery cycled under Condition E. (f) As-prepared LTO/C. (g) LTO/C in fully charged NCM/(LTO/C) battery stored under Condition D. (h) LTO/C in NCM/(LTO/C) battery cycled under Condition E. Note that the NCM/LTO and NCM/(LTO/C) batteries tested under Conditions D and E were fully discharged before the XRD analysis.

(Fig. 3b). Based on the above analysis, the components and the thickness of the SEI film formed at the surface of LTO under Condition B are quite different from that subjected to Condition A. With the exception of the decomposition products of solvents, Li$_2$TiF$_6$ and LiF formed on LTO under Condition B can further separate the LTO from the surrounding solvents thereby leading to an obviously less reactivity of LTO in electrolyte solution than in LIPF$_6$-free solvents.

After NCM/LTO batteries were subjected to storage and cyclic tests (Conditions D and E), similar gassing behaviors were found as expected. The (111) plane at the outermost surface of LTO transforms to (222) plane, which is covered by a thin SEI film formed by the products derived from the interfacial reaction between LTO and electrolyte solution when LTO batteries were subjected to Conditions D and E (Fig. 3e–f). The thicknesses of the phase-change layers (from (111) to (222) plane) for LTOs under both conditions (storage and cyclic test) are almost the same (~3 nm), which are, interestingly, similar to that of the LTO soaked under Condition A. It is thought that the phase-change occurs only in a very thin surface layer (~3 nm). As discussed above, the phase change is attributed to the loss of Li$^+$ and O^{2-} ions from the (111) plane by the interfacial reactions between LTO and electrolyte solution. Both the phase-change surface along with newly formed (222) plane and the SEI film formed on top of the phase-change surface become the barrier to separate the LTO from the surrounding electrolyte solution, which can restrain the further interfacial reactions and loss of Li$^+$ and O^{2-} ions from the interior part of LTO. Therefore, it is said that the interfacial reactions between LTO and electrolyte solution mainly occur at the early stage of the storage or cyclic test. As such, the gassing rate gradually decreases as storage and cyclic test continue.

The XRD patterns show that the LTO electrodes tested under Condition D or E maintain the original spinel structure (Supplementary Fig. S8c). However, the XPS (Ti 2p and O 1s) spectra offer no information for unreacted LTO, a strong evidence of the reacted LTO particles being covered completely by the SEI film of reaction products (Supplementary Fig. S5d–e and S5i–j). The detailed XPS results (C 1s) and FTIR spectra indicate that the C-O species are the main components of the SEI film on LTO after storage and cyclic test, which is similar to that of LTO soaked under Condition B (Supplementary Figs S5m–o and S6e–f).

However, it should be mentioned that the formation mechanism of SEI film on LTO electrode is totally different from that on graphite anode. The formation of SEI film on graphite anode is attributed to the reduction reaction of electrolyte solution (~0.7 V) along with gassing and Li$_2$CO$_3$ and ROCO$_2$Li are the main components[44,45]. Because the reduction potential of most solvents is ~0.7 V, the

reduction reaction of electrolyte solution occurs rapidly when the graphite anode is discharged to below 0.7 V. Thus, the formation of SEI film only occurs in the first several cycles during the battery formation and stops in the following cycling. After formation, the gassing behavior stops in the graphite anode battery due to a stable and complete SEI film can separate the graphite from electrolyte solution and suppress the reduction decomposition of electrolyte.

In contrast, the formation of SEI film on LTO is resulted from the interfacial reactions between LTO and electrolyte solution, not the reduction of the electrolyte solution. The rate of interfacial reactions in LTO batteries is much lower than that of the reduction reaction of electrolyte solution in graphite-based batteries, and therefore a complete SEI film cannot be formed on LTO electrode during the battery formation process like the case of graphite electrode. Thus, the interfacial reaction further occurs during battery cycling test and long-term storage, which results in the continuous gas-release. The SEI film on LTO electrode is formed gradually with the processing of interfacial reaction, which leads to the decrease in the continuous gassing rate of LTO based battery accordingly. Moreover, the SEI film formed on the surface of LTO after the cyclic test under Condition E is much thicker than that LTO after storage under Condition D. It is well-known that the electrolyte solution is consumed during the battery cyclic tests gradually increasing the SEI film thickness.

Gases such as H_2, CO_2 and CO were generated under both Conditions D and E. CO_2 is derived from the decarboxylation reactions of solvents, similarly to Conditions A and B. As discussed above, H_2 does not arise from the reactions of Li ions (or lithium metal) with H_2O (or HF). The alkyl groups in alkyl carbonate are the only species that can provide the H proton in the battery. Therefore, the dehydrogenation of the alkoxy group in solvents may be promoted by LTO subjected to charge/discharge cycles and are responsible for the generation of H_2. The intermediates of solvent dehydrogenation can further accept electrons and Li ions leading to the decarbonylation reactions and generation of CO[46]. The possible reaction mechanism is described in Figure 4c. CO_2 can also be reduced to form CO according to Figure 4d[33,46–48]. Therefore, it can be concluded that the LTO electrodes induce decarbonylation, decarboxylation and dehydrogenation reactions of solvents, directly accountable for gassing in LTO batteries.

Carbon coating around LTO is found as an effective method to suppress the gassing behavior of NCM/LTO batteries. The d-spacing measured from the HRTEM image of the as-prepared LTO/C is 0.481 nm (Fig. 3g), which matches well with the (111) plane of spinel LTO. The HRTEM images suggest that the LTO surface (e.g. the (111), (222) and (400) planes) is covered by a ~5 nm thick carbon layer (Fig.3g and Supplementary Fig. S3d–e).

The XRD patterns of LTO/C after cyclic and storage tests (Conditions D and E) indicate the formation of LiF, which was absent in the cases of the uncoated LTO electrode as discussed above (Fig. 5d–e and 5g–h). The formation of LiF as an important SEI component is thought to be the consequence of the reaction between PF_5 and Li_2CO_3 that is easily formed on the coated carbon surface during the battery first charge/discharge cycle, as reported previously[44], and can stabilize the interface of carbon and electrolyte. In addition, the electric conductance of electrode is highly improved by the coating carbon. It is well-known that the formation of SEI film requires many electrons for decomposition of electrolyte solution. Thus, the high conductance of coating carbon favors an excellent and complete SEI formation, which can further protect the LTO from interfacial reactions.

The XPS spectra (O 1s and C 1s) and FTIR spectra of LTO electrodes indicate that the RCO_3Li, C-O-C, and ROLi species in the SEI film were formed on the surface of LTO/C after battery storage (Condition D) and cyclic test (Condition E) (Supplementary Figs. S6h–i and S10g–h and k–l). That is, the carbon coating together with

the stable SEI film formed on top of the carbon coating as a barrier layer may offer significant synergy to protect the LTO electrode from the surrounding electrolyte solution, eliminating the possible interfacial gassing reaction[49].

The HRTEM images exhibited that the morphologies of the interface between LTO and carbon coating hardly changed under Conditions D and E , proving a stable interface existing between them (Fig. 3h–i). Therefore, it can be said that carbon coating is an effective strategy to fully suppress the interfacial reaction and gassing on the LTO surface.

In summary, the gassing phenomenon in LTO electrodes has been one of the most serious obstacles to their large-scale applications in LIBs. PF_5, as a strong Lewis acid of decomposition product of $LiPF_6$, has been erroneously regarded as a major source for gassing in the presence of trace amount of water. This paper clarifies that the gassing reactions, including decarboxylation, decarbonylation and dehydrogenation reactions of solvents, are initiated not by PF_5, but by LTO on the outermost surface of LTO (111) plane. The interfacial reactions between LTO and electrolyte solution generate gasses like H_2, CO_2 and CO, which are the main sources for swelling of battery pack. The gassing involves the plane transformation of LTO from (111) to (222) and the formation of (101) plane of anatase TiO_2 and the outermost surface Li^+ and O^{2-} ions of the LTO (111) plane are removed from LTO by the interfacial reactions.

Constructing a barrier layer is an effective strategy to control the interfacial reactions between LTO and the surrounding electrolyte solution, and a nanoscale carbon coating on LTO is proven to suppress the gassing of LTO batteries. The coated carbon, together with the stable SEI film formed around the coating offer significant synergy to separate LTO from the surrounding electrolyte solution and prevent the interfacial gassing reactions. The modification of LTO surface is a simple yet very effective strategy, which can both improve the high-rate charge/discharge performance of batteries and suppress the gassing behavior of LTO battery.

Methods

Synthesis of rutile TiO_2, LTO and LTO/C. Rutile TiO_2 was obtained by sintering the precursor amorphous TiO_2 at 900°C for 8 h. The LTO powder was synthesized by solid-state reaction of the mixture containing amorphous TiO_2 with Li_2CO_3 in air. The TiO_2 and Li_2CO_3 were mixed at a Li:Ti molar ratio of 4.2:5. Carbon coated LTO (LTO/C) composites were also prepared based on a similar solid-state reaction using the precursor mixture plus glucose in argon atmosphere. The details of the synthesis route can be found elsewhere[49,50].

Preparation of soft-packed NCM/LTO batteries. Commercial 034352 type soft packed NCM/LTO batteries, of dimensions 3 mm thick, 43 mm wide and 52 mm long, were assembled to investigate the gassing behaviors of LTO batteries. The batteries were made of $Li(Ni_{1/3}Co_{1/3}Mn_{1/3})O_2$ (NCM) (Tianjiao Technology, Shenzhen, China) as the cathode, as- prepared LTO or LTO/C as the anode, polyethylene as the separator, and 1 M $LiPF_6$/EC+DMC+EMC as the electrolyte solution. The NCM cathode consisted of 85 wt.% NCM, 9 wt.% Super-P and 6 wt.% poly(vinylidene fluoride)(PVDF) binder, whereas the LTO anode consisted of 80 wt.% LTO, 10 wt.% Super-P and 10 wt.% PVDF. These components were rolled together to form the battery core and assembled into aluminum-plastic laminated film packages. Batteries were charged and discharged three times between 1.5 and 2.8 V at a rate of 0.5C for stabilization before storage and cyclic tests under Conditions D and E.

Gassing behaviors (Conditions A–E). As demonstrated in Table 1, five different conditions were designed to clarify the root causes of the gassing behaviors and the gases generated under all these conditions were analyzed on a gas chromatograph (Agilent 7890A GC System) using the GB/T 9722-2006 method.

Conditions A and B: LTO (or rutile TiO_2) soaked in electrolyte-free solvent or electrolyte solution. 1.6 g of LTO or rutile TiO_2 powders was put into aluminum-plastic laminated film packages, and 4 mL $LiPF_6$-free solvent or $LiPF_6$-based electrolyte solution was added before sealing of the packages in an argon-filled glove box (See Table 1 for details of the solvents and electrolytes used). The electrode packages were stored at 25 or 50°C for 3 months. The volumes of the packages before and after storage were monitored using the water displacement method.

Condition C. Electrolyte solution (1 M $LiPF_6$/EC+DMC+EMC) stored at 25 or 50°C for 3 months in the absence of LTO. This condition is designed to evaluate the role of $LiPF_6$ in the gassing reactions.

Condition D: Storage test of soft-packed NCM/LTO or NCM/(LTO/C) batteries. The assembled fully charged batteries were stored at 25°C for 3 months.

Condition E: Cyclic test of soft-packed NCM/LTO or NCM/(LTO/C) batteries. The assembled batteries were measured for 400 cycles at a charge/discharge rate of 0.5C (0.5C/0.5C) at 25°C.

Characterization of structure and morphology changes of LTO and LTO/C under different conditions. The LTO and LTO/C electrode materials were rinsed after tests using DMC to remove the electrolyte and dried in the glove box antechamber to remove the residual DMC. XRD patterns of the samples were obtained on a diffractometer (Rigaku D/max 2500/PC) using Cu Kα radiation. The morphologies were examined using a TEM (JOEL JEM-2100F, Japan). XPS measurements were conducted using Physical Electronics PHI5802 instrument using X-rays magnesium anode (monochromatic Kα X-rays at 1253.6 eV) as the source. The C 1s region was used as a reference and was set at 284.8 eV.

1. Tarascon, J.-M. & Armand, M. Issues and challenges facing rechargeable lithium batteries. *Nature* **414**, 359–367 (2001).
2. Dunn, B., Kamath, H. & Tarascon, J. M. Electrical Energy Storage for the Grid: A Battery of Choices. *Science* **334**, 928–935 (2011).
3. Kaskhedikar, N. A. & Maier, J. Lithium Storage ion Carbon Nanostructures. *Adv. Mater.* **21**, 2664–2680 (2009).
4. Liu, C., Li, F., Ma, L. P. & Cheng, H. M. Advanced Materials for Energy Storage. *Adv. Mater.* **22**, E28–E62 (2010).
5. Spotnitz, R. & Franklin, J. Abuse behavior of high-power, lithium-ion cells. *J. Power Sources* **113**, 81–100 (2003).
6. Jung, H. G., Jang, M. W., Hassoun, J., Sun, Y. K. & Scrosati, B. A high-rate long-life $Li_4Ti_5O_{12}/Li[Ni_{0.45}Co_{0.1}Mn_{1.45}]O_4$ lithium-ion battery. *Nat. Commun* **2** (516), 511–515 (2011).
7. Kang, K. S., Meng, Y. S., Breger, J., Grey, C. P. & Ceder, G. Electrodes with high power and high capacity for rechargeable lithium batteries. *Science* **311**, 977–980 (2006).
8. Amine, K. *et al.* Nanostructured Anode Material for High-Power Battery System in Electric Vehicles. *Adv. Mater.* **22**, 3052–3057 (2010).
9. Ferg, E., Gummow, R. J., Kock, A. d. & Thackeray, M. M. Spinel Anodes for Lithium-Ion Batteries. *J. Electrochem. Soc.* **141**, L147–L150 (1994).
10. Ohzuku, T., Ueda, A. & Yamamoto, N. Zero-Strain Insertion Material of $Li[Li_{1/3}Ti_{5/3}]O_4$ for Rechargeable Lithium Cells. *J. Electrochem. Soc.* **142**, 1431–1435 (1995).
11. Aldon, L. *et al.* Chemical and Electrochemical Li-Insertion into the $Li_4Ti_5O_{12}$ Spinel. *Chem. Mater.* **16**, 5721–5725 (2004).
12. Li, B. H. *et al.* Facile synthesis of $Li_4Ti_5O_{12}$/C composite with super rate performance. *Energy Environ. Sci.* **5**, 9595–9602 (2012).
13. Zhao, L., Hu, Y. S., Li, H., Wang, Z. X. & Chen, L. Q. Porous $Li_4Ti_5O_{12}$ Coated with N-Doped Carbon from Ionic Liquids for Li-Ion Batteries. *Adv. Mater.* **23**, 1385–1388 (2011).
14. Wang, G. J. *et al.* Preparation and characteristic of carbon-coated $Li_4Ti_5O_{12}$ anode material. *J. Power Sources* **174**, 1109–1112 (2007).
15. Zhu, G.-N. *et al.* Carbon-coated nano-sized $Li_4Ti_5O_{12}$ nanoporous micro-sphere as anode material for high-rate lithium-ion batteries. *Energy Environ. Sci.* **4**, 4016–4022 (2011).
16. Park, K. S., Benayad, A., Kang, D. J. & Doo, S. G. Nitridation-Driven Conductive $Li_4Ti_5O_{12}$ for Lithium Ion Batteries. *J. Am. Chem. Soc.* **130**, 14930–14931 (2008).
17. Ji, S. Z. *et al.* Preparation and effects of Mg-doping on the electrochemical properties of spinel $Li_4Ti_5O_{12}$ as anode material for lithium ion battery. *Mater. Chem. Phys.* **123**, 510–515 (2010).
18. Tian, B., Xiang, H., Zhang, L., Li, Z. & Wang, H. Niobium doped lithium titanate as a high rate anode material for Li-ion batteries. *Electrochim. Acta* **55**, 5453–5458 (2010).
19. Huang, S. H., Wen, Z. Y., Zhu, X. J. & Gu, Z. H. Preparation and electrochemical performance of Ag doped $Li_4Ti_5O_{12}$. *Electrochem. Commun.* **6**, 1093–1097 (2004).
20. Li, X., Qu, M. Z., Huai, Y. J. & Yu, Z. L. Preparation and electrochemical performance of $Li_4Ti_5O_{12}$/carbon/carbon nano-tubes for lithium ion battery. *Electrochim. Acta* **55**, 2978–2982 (2010).
21. Li, X., Qu, M. Z. & Yu, Z. L. Preparation and electrochemical performance of $Li_4Ti_5O_{12}$/graphitized carbon nanotubes composite. *Solid State Ionics* **181**, 635–639 (2010).
22. Cai, R., Yu, X., Liu, X. & Shao, Z. $Li_4Ti_5O_{12}$/Sn composite anodes for lithium-ion batteries: Synthesis and electrochemical performance. *J. Power Sources* **195**, 8244–8250 (2010).
23. Zhang, B. *et al.* Urchin-like $Li_4Ti_5O_{12}$-carbon nanofiber composites for high rate performance anodes in Li-ion batteries. *J. Mater. Chem.* **22**, 12133–12140 (2012).
24. Borghols, W. J. H., Wagemaker, M., Lafont, U., Kelder, E. M. & Mulder, F. M. Size Effects in the $Li_{4+x}Ti_5O_{12}$ Spinel. *J. Am. Chem. Soc.* **131**, 17786–17792 (2009).
25. Zhu, G. N., Wang, Y. G. & Xia, Y. Y. Ti-based compounds as anode materials for Li-ion batteries. *Energy Environ. Sci.* **5**, 6652–6667 (2012).
26. Belharouak, I. *et al.* Performance Degradation and Gassing of $Li_4Ti_5O_{12}/LiMn_2O_4$ Lithium-Ion Cells. *J. Electrochem. Soc.* **8**, A1165–A1170 (2012).
27. Wu, K., Yang, J., Zhang, Y., Wang, C. & Wang, D. Investigation on $Li_4Ti_5O_{12}$ batteries developed for hybrid electric vehicle. *J Appl Electrochem.* DOI 10.1007/s10800-012-0442-0 (2012).
28. Yang, Z. *et al.* Electrochemical Energy Storage for Green Grid. *Chem. Rev.* **111**, 3577–3613 (2011).
29. Hammouche, A., Karden, E., Walter, J. & Doncker, R. W. D. On the impedance of the gassing reactions in lead-acid batteries. *J. Power Sources* **96**, 106–112 (2001).
30. Du Pasquier, A., Plitz, I., Menocal, S. & Amatucci, G. A comparative study of Li-ion battery, supercapacitor and nonaqueous asymmetric hybrid devices for automotive applications. *J. Power Sources* **115**, 171–178 (2003).
31. Ding, Z. J. *et al.* Towards understanding the effects of carbon and nitrogen-doped carbon coating on the electrochemical performance of $Li_4Ti_5O_{12}$ in lithium ion batteries: a combined experimental and theoretical study. *PCCP* **13**, 15127–15133 (2011).
32. Lu, X. *et al.* Lithium Storage in $Li_4Ti_5O_{12}$ Spinel: The Full Static Picture from Electron Microscopy. *Adv. Mater.* **24**, 3233–3238 (2012).
33. Xu, K. Nonaqueous liquid electrolytes for lithium-based rechargeable batteries. *Chem. Rev.* **104**, 4303–4417 (2004).
34. Sloop, S. E., Pugh, J. K., Wang, S., Kerr, J. B. & Kinoshita, K. Chemical Reactivity of PF_5 and $LiPF_6$ in Ethylene Carbonate/Dimethyl Carbonate Solutions. *Electrochem. Solid-State Lett.* **4**, A42–A44 (2001).
35. Sloop, S. E., Kerr, J. B. & Kinoshita, K. The role of Li-ion battery electrolyte reactivity in performance decline and self-discharge. *J. Power Sources* **119–121**, 330–337 (2003).
36. Wang, Y.-Q. *et al.* Rutile-TiO_2 Nanocoating for a High-Rate $Li_4Ti_5O_{12}$ Anode of a Lithium-Ion Battery. *J. Am. Chem. Soc.* **134**, 7874–7879 (2012).
37. Leroy, S., Martinez, H., Dedryvere, R., Lemordant, D. & Gonbeau, D. Influence of the lithium salt nature over the surface film formation on a graphite electrode in Li-ion batteries: An XPS study. *Appl. Surf. Sci.* **253**, 4895–4905 (2007).
38. Dedryvere, R. *et al.* Electrode/Electrolyte Interface Reactivity in High-Voltage Spinel $LiMn_{1.6}Ni_{0.4}O_4/Li_4Ti_5O_{12}$ Lithium-Ion Battery. *J Phys Chem C* **114**, 10999–11008 (2010).
39. Dedryvere, R. *et al.* Characterization of lithium alkyl carbonates by X-ray photoelectron spectroscopy: Experimental and theoretical study. *J. Phys. Chem. B* **109**, 15868–15875 (2005).
40. Janz, G. J., Lorenz, M. R. & Brown, C. T. Preparation and Thermal Stability of Lithium Titanium Fluoride. *J. Am. Chem. Soc.* **80**, 4126–4128 (1958).
41. Alfarra, A., Frackowiak, E. & Beguin, F. Mechanism of lithium electrosorption by activated carbons. *Electrochim. Acta* **47**, 1545–1553 (2002).
42. Zhang, J. H., Maurer, F. H. J. & Yang, M. S. In situ Formation of TiO_2 in Electrospun Poly(methyl methacrylate) Nanohybrids. *J Phys Chem C* **115**, 10431–10441 (2011).
43. Dedryvere, R. *et al.* XPS identification of the organic and inorganic components of the electrode/electrolyte interface formed on a metallic cathode. *J. Electrochem. Soc.* **152**, A689–A696 (2005).
44. Dedryvère, R. *et al.* Surface film formation on electrodes in a $LiCoO_2$/graphite cell: A step by step XPS study. *J. Power Sources* **174**, 462–468 (2007).
45. Wang, Y. X., Nakamura, S., Ue, M. & Balbuena, P. B. Theoretical studies to understand surface chemistry on carbon anodes for lithium-ion batteries: Reduction mechanisms of ethylene carbonate. *J. Am. Chem. Soc.* **123**, 11708–11718 (2001).
46. Yoshida, H. *et al.* Degradation mechanism of alkyl carbonate solvents used in lithium-ion cells during initial charging. *J. Power Sources* **68**, 311–315 (1997).
47. Aurbach, D. *et al.* The Correlation between the Surface-Chemistry and the Performance of Li-Carbon Intercalation Anodes for Rechargeable Rocking-Chair Type Batteries. *J. Electrochem. Soc.* **141**, 603–611 (1994).
48. Aurbach, D., Markovsky, B., Weissman, I., Levi, E. & Ein-Eli, Y. On the correlation between surface chemistry and performance of graphite negative electrodes for Li ion batteries. *Electrochim. Acta* **45**, 67–86 (1999).
49. He, Y. B. *et al.* Carbon coating to suppress the reduction decomposition of electrolyte on the $Li_4Ti_5O_{12}$ electrode. *J. Power Sources* **202**, 253–261 (2012).
50. Ning, F. *et al.* Effects of TiO_2 crystal structure on the performance of $Li_4Ti_5O_{12}$ anode material. *J. Alloys Compd.* **513**, 524–529 (2012).

Acknowledgements

Author contributions

Q.-H.Y. and F.Y.K. conceived the project and Y.-B.H., B.H.L. and Q.-H.Y. designed the experiments. Y.-B.H. B.H.L. and M.L. carried out the materials synthesis, battery assembly

Additional information